Effect of pre-strain on hydrogen-induced delayed cracking for medium Mn steels

Q.Y. Liu[a], Y. Yan[a,*], Q.J. Zhou[b], S.Q. Yang[a], J.X Li[a], Y.J. Su[a] , L.J. Qiao[a]

[a] Beijing Advanced Innovation Center for Materials Genome Engineering, Corrosion and Protection Center, Key Laboratory for Environmental Fracture (MOE), Institute for Advanced Materials and Technology, University of Science and Technology Beijing, 100083, China
[b] Baoshan Iron & Steel Co., Ltd, Research Institute, Shanghai 201900, China

***corresponding author.**
E-mail address: yanyu@ustb.edu.cn (Y. Yan).

Abstract

Medium Mn steels are a class of the new-generation ultra-high-strength materials used in automotives. However, despite excellent ductility, they may suffer from delayed cracking and thus cause serious concerns. In this study, several medium Mn steels were tested with different prestrain and hydrogen charging conditions. The interaction and synergistic effects of prestrain and hydrogen content on hydrogen-induced delayed cracking behavior are investigated. The threshold stress of hydrogen-induced cracking (HIC) decreased during dynamic hydrogen charging under a constant load. In the process of dynamic hydrogen charging, for M7B and M10B steels, the normalized stress intensity factor σ/σ_b and the corresponding threshold stress rHIC decreased sharply as prestrain increased. This is because the volume fraction of retained austenite decreased with an increase in prestrain. Similarly, rHIC was reduced and the critical hydrogen content dropped drastically with increasing prestrain. For M7C, the influence of prestrain on threshold stress and hydrogen concentration was less than that of M7B. This is because the different treatment processes leads to a different stability of the retained austenite. By observing the SEM fractographs, the fracture surface of medium Mn steels showed different fracture characteristics, such as dimple fractures and intergranular and transgranular modes.

Key words:

Medium Mn steel, Constant load test, Dynamic hydrogen charging,

Fracture morphology, Pre-strain

1. Introduction

With the rapid development of vehicles, weight-lightening, energy-saving and safety-improvement are urgently required in the automobile industry. In the past, the main consideration of automobile manufacturers was the cost, formability and corrosion resistance of advanced high strength steels (AHSSs) with typically multiphase microstructures. As the strength of the material increases, however the sensitivity to hydrogen-induced delayed cracking is also increased during its production, processing, and actual environmental service. Delayed cracking is an environmental embrittlement resulting from the interaction of the material's environmental stress, which limits its application in the field of high-end manufacturing equipment. As is known, hydrogen damage, such as hydrogen bubbling and hydrogen cracking, would appear in steels when the hydrogen concentration reaches or exceeds a critical value. The existence of internal and external stress promotes the diffusion and enrichment of atomic hydrogen, decreasing its ductility. This phenomenon is called hydrogen-induced ductility loss or hydrogen embrittlement. When accompanied with constant load, the enrichment of atomic hydrogen promotes the nucleation and spread of hydrogen cracking. This mechanism is called hydrogen-induced delayed cracking (HIDC).

Medium Mn steels (MMSs), with 4~10wt% Mn [1], have become the typical steel used in automobiles. Mn[1, 2] promotes austenite formation to increase the volume fraction of retained austenite (RA) in medium Mn steel at room tempreture, resulting in the good ductility of MMSs. Because of this, it is generally not possible to crack MMSs by cold working. When, however, the material is exposed to the service environment, hydrogen will adsorb and diffuse to the interior of the material, which has a serious impact on its properties.[3] The high strength of medium Mn steel (1000~1600MPa) is easily susceptible to hydrogen embrittlement (HE) [4]. Hydrogen-enhanced localized plasticity (HELP) [5], hydrogen-enhanced decohesion (HEDE) [6] and hydrogen-enhanced and strain-induced vacancies (HESIV) [7, 8] explain the mechanism of HE. Some researchers have studied the sulphur content and inclusion distribution[9], and the correlation between hydrogen-induced stress and hydrogen embrittlement [10] under constant load. A reliable method to evaluate the sensitivity of HIDC is the constant load test. In this study, we systematically investigated how hydrogen influenced delayed cracking and the relationship between hydrogen, pre-strain and critical stress.

The size of the austenite and the partition of Mn to austenite during the intercritical annealing process were the two main contributors to austenite stability [11]. In general, at room temperature in 6 mass% Mn steel, the partitioning of Mn in austenite grains was sufficient to stabilize the retained austenite. External pre-strain, dislocations and internal stress due to martensitic transformation are expected to exert

influences on medium Mn steels[12]. Pre-strain for medium Mn steels can enhance its strength and reduce its ductility. In this study, we investigated systematically the interaction between pre-strain and dynamic hydrogen charging in MMSs.

2. Experimental details

Materials

The medium Mn steel (MMS) thin plates were supplied by Baoshan Iron&Steel Co., Ltd.

In this study, the effect of pre-strain on hydrogen-induced delayed cracking of MMSs was investigated. The main differences between the three kinds of manganese steels are the Mn content and the heat treatment process[13].

The heat treatment detail involved hot-rolled, intercritically batch-annealed, and cold-rolled as follows. The slabs after steelmaking were heated to 1473K for 2 hours and hot-rolled with a temperature of 1153 K. The intercritical batch annealing was conducted at 893 K for 12 hours. The thickness for hot-rolled sheets was 2.8mm, consisting of austenite and ferrite. Then the sheets were pickled and cold-rolled to a thickness of 1.4mm and the thickness conduction was 50pct. The cold-rolled medium Mn steel sheets were heated to 893 K and held for 3 minutes and 12 hours. The annealing time is relevant to continuous annealing and batch annealing processes, respectively.

Table **1** lists the chemical composition of the material The samples prepared in these two annealing conditions are designated as “M7B”, “M7C” and “M10B” respectively, ‘M’ referring to Mn, ‘7’ or ‘10’ meaning the content of Mn, ‘B’ for batch annealing and ‘C’ for continuous annealing. Transmission electron microscope (TEM) and scanning electron microscopy (SEM) were used to observe the microstructure and fracture morphology.

Table 1 Chemical composition in wt. % of MMSs

Material/element	C	Si	Mn	Cr	Al	Fe
M7B	**0.14**	**0.23**	**7.16**	**0.077**	**0.055**	**balance**
M7C	**0.14**	**0.23**	**7.14**	**0.082**	**0.056**	**balance**
M10B	**0.15**	**0.17**	**10.40**	**0.073**	**1.49**	**balance**

Immersion test

Hydrogen concentration was measured using the G4 Phoenix DH diffusion hydrogen analyser. The G4 hydrogen detector collects hydrogen from the sample by

means of an overheating extraction method. The sample is heated by infrared heating, and the hydrogen inside the specimen escapes selectively according to the temperature. The gas carried by the carrying nitrogen is detected by the thermal conductivity detector. Hydrogen concentration was measured by G4 at 800℃ for 20 min.

A 20% NH_4SCN solution was selected for the immersion test, and the ratio of the solution volume to the sample area was 7.8 ml/cm^2. Since it is more moderate than a HCl solution, it causes weaker corrosion on the surface. Therefore, it is often used as soaking hydrogen to evaluate the susceptibility of hydrogen embrittlement (SHE).

With a size of 15×5mm2, the sample was sanded to 800 grits, ultrasonically cleaned and dried. The sample was soaked in the 20% NH4SCN solution and taken out at the prescribed time. The surface was washed with alcohol to remove surface corrosion deposits. After drying and weighing, the hydrogen content was measured in the G4 hydrogen analyser. In order to avoid the escaping of diffused hydrogen, the cleaning and drying time is controlled within three minutes. Due to the dispersion of experimental data for the hydrogen test, the average value of three samples is generally used. Multiple parallel samples were measured at critical data points.

Constant load test

The constant load test (CLT) is a reliable method to evaluate the sensitivity of hydrogen-induced delayed cracking. Some researchers have determined the critical hydrogen concentration for the delayed fracture of high-strength steel by CLT [14].

The sample prepared for CLT was placed in the solution for dynamic electrochemical hydrogen charging. In order to facilitate clamping, a circular hole was machined on both sides of the sample. Its specific dimensions are shown in Fig. 1. The gauge of the sample was 20mm long, 5mm wide and approximately 1.5mm thick, and its surface was wet-grounded up to 2000 grit with SiC paper, and then ultrasonically cleaned in acetone and ethanol. The tensile direction was parallel to the rolling direction. Only the gauge part of the sample was charged, because other parts were sealed by silica gel. A 0.1mol/L H_2SO_4+0.22g/L of thiourea was used as the hydrogen charging solution, where thiourea could be used as a poison to improve hydrogen charging efficiency. DH1719A-5 DC stabilised current supply was chosen as the hydrogen charging power. The sample was used as the cathode and the platinum wire as the anode, while the hydrogen charging current density was 1mA/cm^2. The specimens were treated with different degrees of pre-strain, and then tensile tests were carried out under different constant loads. Considering the experimental cycle and accuracy, the cut-off time was 200 hours.

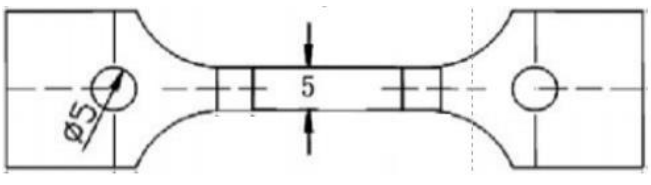

Fig.1 Specimen size for constant load (72mm long and 18mm wide): mm

The electrochemical hydrogen charging was conducted while exerting constant load. After sufficient time, the local hydrogen concentration Cσ at maximum stress can be given by the following formula:

$$C\sigma = C_0 (\alpha V_H \sigma / RT) \quad (1)$$

where α is the stress concentration factor, related to the inclusion shape. The applied stress brought the stress concentration close to impurity or second phase. Cσ increases with increasing applied stress. When C_σ reaches the critical hydrogen concentration of C_{th}, the hydrogen induced crack begins to nucleate and propagate, causing macroscopic delayed cracking. At this point, the applied stress corresponds to the threshold stress value of hydrogen induced delayed cracking, σ_{HIC}.

In order to measure the hydrogen-induced delayed cracking threshold stress σ_{HIC}, the sample was charged under the same hydrogen charging current density with a cut-off time of 200 hours. Exerting different loads by different methods and recording the fracture time of each specimen, t_F, σ_y and σ_n were found to be the minimum applied loads causing cracking and the maximum loads that did not cause cracking within the given time. Then, the threshold stress value σ_{HIC} can be calculated by the following formula.

$$\sigma_{HIC} = (\sigma_y + \sigma_n) / 2 \text{ and } (\sigma_y - \sigma_n) \leq 0.1 (\sigma_y + \sigma_n) \quad (2)$$

In order to ensure that the error of the measured threshold stress is less than 10%, Eq.(2) must be satisfied [10]. When the applied stress σ approaches σ_{HIC}, delayed cracking occurs after a period of time. At present, the average hydrogen concentration of C_0 is measured by G4, and the average hydrogen concentration is theoretically lower than the critical hydrogen concentration.

3. Results and discussion

Microstructure and mechanical properties

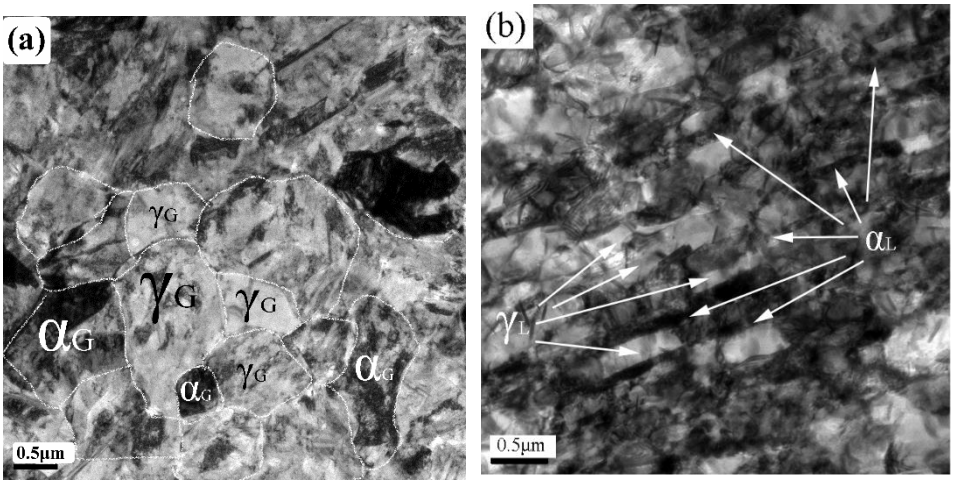

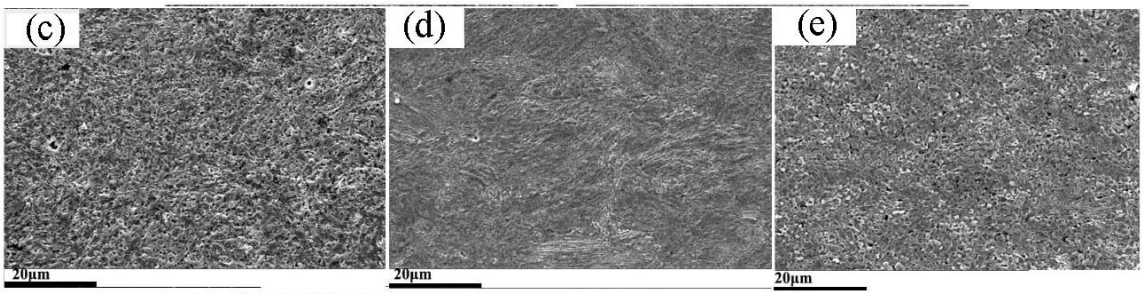

Fig. 2 TEM micrographs of (a)M7B and(b) M7C and SEM image of (c)M7B (d)M7C (e)M10B, respectively. α_L and γ_L are lath-shaped ferrite and retained austenite, α_G and γ_G are globular-shaped ferrite and retained austenite.

Fig. 2 presents the SEM and TEM images of test steels. In Figs 2(c)(d)(e), M7B and M10B show black spots, while M7C is distributed in black strip. The convex and concave parts in the SEM micrograph of MMSs represent ferrite and retained austenite, respectively. Due to the ultrafine grained size of test steel, TEM is used to discern the grain and phase structure more clearly. As is known, MMSs have a dual phase of ferrite and retained austenite. In Figs 2(a)(b), M7B and M10B are uniformly distributed with globular-shaped ferrite and retained austenite, and a grain size of about 1–3μm. The microstructure of M7C is mainly distributed with lath-shaped austenite and ferrite, which is mainly due to incomplete annealing. Lengthy batch annealing leads to the full recrystallisation of martensite while it reverts to austenite. And long strip austenite can be combined into block austenite. Continuous annealing for 1-3 minutes can promote the transformation of martensite to austenite, but its microstructure still retains the characteristics of lath martensite.

Austenite plays a key role in this transformation. The transformation of austenite to martensite will be triggered when deformation occurs [15]. Previous studies have provided evidence that the stability of austenite depends on the grain size of austenite [16, 17]. The ultrafine-grained austenite grain acts as an obstacle towards the motion of dislocations which were generated during the nucleation of martensite [18].

The mechanical properties of MMSs, after different annealing processes, are shown in Table 2. Elongation was measured by the gauge line. The steels exhibit an excellent combination of high strength and ductility. For example, M7B scores 745MPa for yield stress, 1133MPa for tensile strength and about 31% of total elongation. The product of tensile strength to ductility for M7B is about 35.5GPa%, 34.3GPa% for M7C and 56.1GPa% for M10B. The fracture tensile in air shows a fully ductile mode.

Table 2 Mechanical properties of MMSs

Material	Yield strength /MPa	Tensile strength /MPa	Elongation /%	Product of strength and elongation / GPa•%
M7B	**745**	**1133**	**31.3%**	**35.5**

M7C	**1113**	**1130**	**30.4%**	**34.3**
M10B	**794**	**1403**	**40.0%**	**56.1**

Table 3 The volume fraction of RA for MMSs under different strain

Material	0	0.05	0.10	0.15
M7B	**23.2%**	**12.2%**	**10.9%**	**7.2%**
M7C	**20.0%**	**8.8%**	**6.6%**	**6.3%**
M10B	**44.1%**	**38.2%**	**37.8%**	**25.9%**

X ray diffraction can be used to determine the volume fraction of RA in MMSs. XRD spectra of MMS specimens before the constant load test were analysed. Based on the integrated intensities of the (200)γ, (220)γ, (331)γ, (211)α and (200)α diffraction peaks, the calculation of the volume fraction of retained austenite (RA) was performed. As shown in Table 3, as the strain increased, the volume fraction of RA decreased.

Immersion test

According to the measurement of hydrogen diffusion coefficient [19], the hydrogen immersion time ensuring the uniform distribution of hydrogen in the specimen is 72 hours. In order to eliminate the influence of temperature on the result, the immersion experiment was carried out in a constant temperature water bath. The temperature was set at 30℃. The change of hydrogen concentration according to immersion time was represented visually by marking each data point in a graph. The fitting curve revealed the change of hydrogen concentration as a function of immersion time (Fig. 3). The value in Fig. 3 is the average result for several parallel specimens.

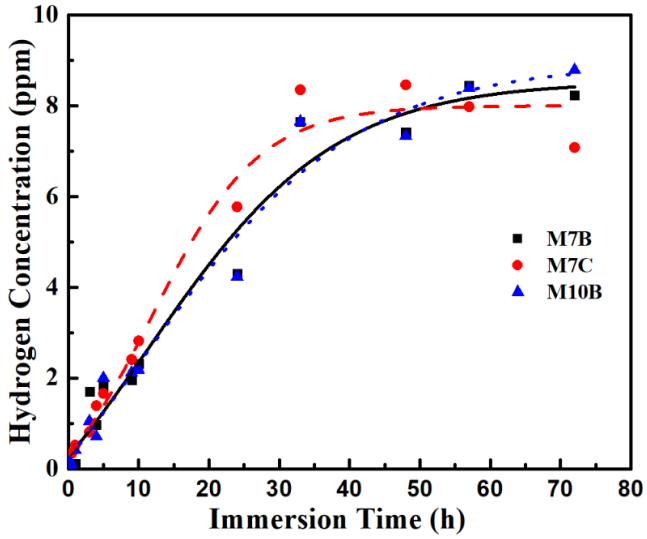

Fig. 3. Hydrogen concentration as function of immersion time

As can be seen from Fig. 3, the hydrogen concentration of MMSs undergoes a rapid change at the early stages, and then reaches a stable value of approximately

8ppm after 50 hours. Since the concentration is far from the saturation of the hydrogen concentration of the specimen itself, it is inferred that this is the highest value that can be reached in the 20% NH_4SCN solution, depending on the hydrogen atom provided by the solution. Therefore, it can be concluded that the hydrogen concentration of MMSs has little impact on the actual service environment, depending on the environment and the load. At the early stages of immersion, the hydrogen concentration of M7C changed faster than that of M7B and M10B. Thus, it can be concluded that morphology is the factor affecting the rate of hydrogen permeation. Hydrogen is more likely to enter the material through the ferrite lath. In the late stages of the experiment, however, the hydrogen concentration in M7C decreased slightly. By observing the material, it was found that its surface had a certain degree of corrosion, indicating that corrosion has a certain impact on hydrogen in the material.

Constant load test (CLT) with dynamic hydrogen charging

The pre-strain amounts of 0, 0.05 and 0.15 for MMSs were obtained, followed by the constant load test with dynamic hydrogen charging. The hydrogen charging current density was 1mA/cm^2 in 0.1mol/L H_2SO_4+0.22g/L thiourea solution. Fig. 4 shows the variation of hydrogen-induced delay fracture time t_F as a function of the normalised stress factor under different pre-strain conditions for all kinds of steels.

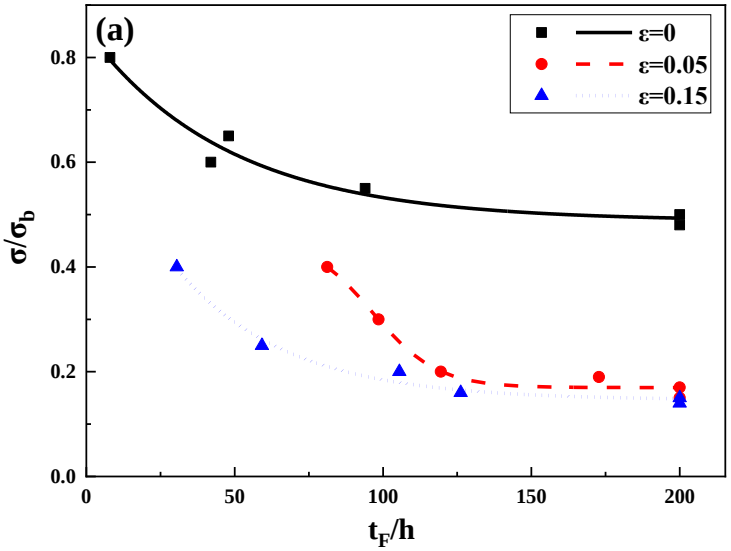

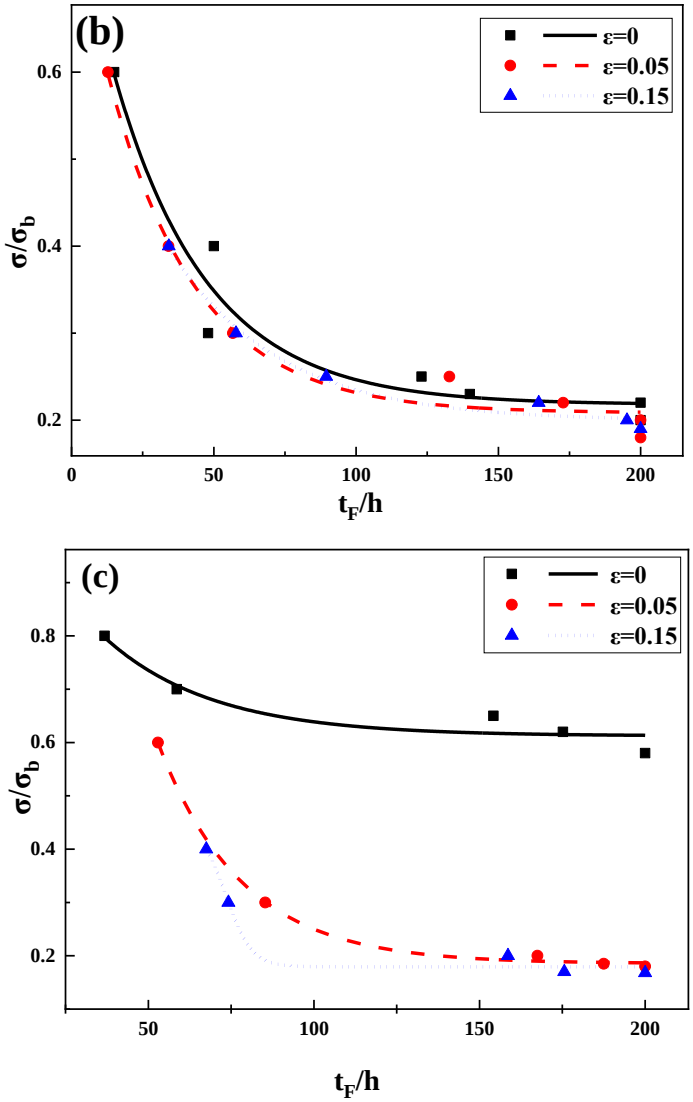

Fig 4 Relation curve between σ/σb and t_F of M7B(a), M7C(b), M10B(c)steel under different pre-strain condition, respectively

According to Eq.(2), the threshold stress value σ_{HIC} of the specimen under different strain conditions can be calculated. As delayed cracking is a combined action of the applied stress and the environment, the result of the CLT is the critical combination of stress and hydrogen charging conditions. Critical hydrogen concentration (Cth) is related to the σ_{HIC}. The concentration of hydrogen induced by stress is difficult to measure. The average hydrogen concentration (C_0) measured near the cut-off time is considered as the critical hydrogen concentration C_{th}. The hydrogen concentration, obtained by G4, as well as the normalised threshold stress are shown in Fig. 5.

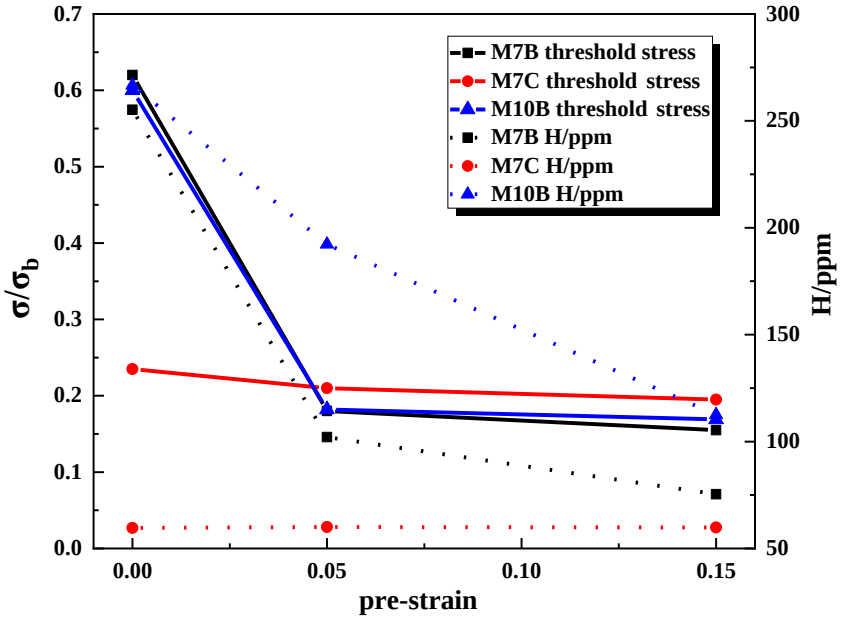

Fig. 5 The normalized threshold stress, σ/σ_b, and hydrogen concentration as function of pre-strain in MMSs

The solid line and dotted line refer to the threshold stress and hydrogen content, respectively.

As can be seen from Fig. 5, for M7B, threshold stress clearly decreases as strain increases. When 0.05 pre-strain was introduced, the normalised threshold stress, σ/σ_b, was sharply reduced from 0.62 to 0.18, while σ/σ_b decreased slightly as the strain continued to increase.

In the process of M7B steel dynamic hydrogen charging, σ/σ_b decreased sharply from 0.62 to 0.155 as the pre-strain increased from 0 to 0.15, and the corresponding σ_{HIC} decreased from 622MPa to 155MPa. Due to the decrease of pre-strain, the volume fraction of RA was decreased, σ_{HIC} reduced and the critical hydrogen content dropped from 255.21ppm to 75.38ppm.

In the process of M7C steel dynamic hydrogen charging, σ/σ_b decreased from 0.235 to 0.195 as the pre-strain increased from 0 to 0.15, and the corresponding σ_{HIC} decreased from 235MPa to 211MPa. Thus, due to the poor stability of RA, the influence of pre-strain on threshold stress was less than that of M7B, causing the normalised threshold stress and the hydrogen concentration to fluctuate slightly with the increase of pre-strain.

In the process of M10B steel dynamic hydrogen charging, σ/σ_b decreased sharply from 0.60 to 0.169 as the pre-strain increased from 0 to 0.15, the corresponding σ_{HIC} decreased from 590MPa to 166Mpa, and the critical hydrogen content dropped from 266.64ppm to 112.53ppm. The properties of M10B are similar to those of M7B under the constant load test. This is because M7B and M10B undergo the same heat treatment process and the stability of RA exhibits similar properties.

The reasons are: (1) hydrogen is easy to accumulate, induced by stress, while its enrichment was weakened by the decrease of threshold stress; (2) the increase of pre-strain reduces the volume fraction of austenite in the material, lessening the

number of hydrogen traps, thus decreasing the solubility of the hydrogen [20, 21].

In addition, the morphology of the specimens under dynamic hydrogen charging CLT was observed by SEM. The macromorphology of each specimen's fracture at low magnification was observed first, and some regions were observed at high magnification.

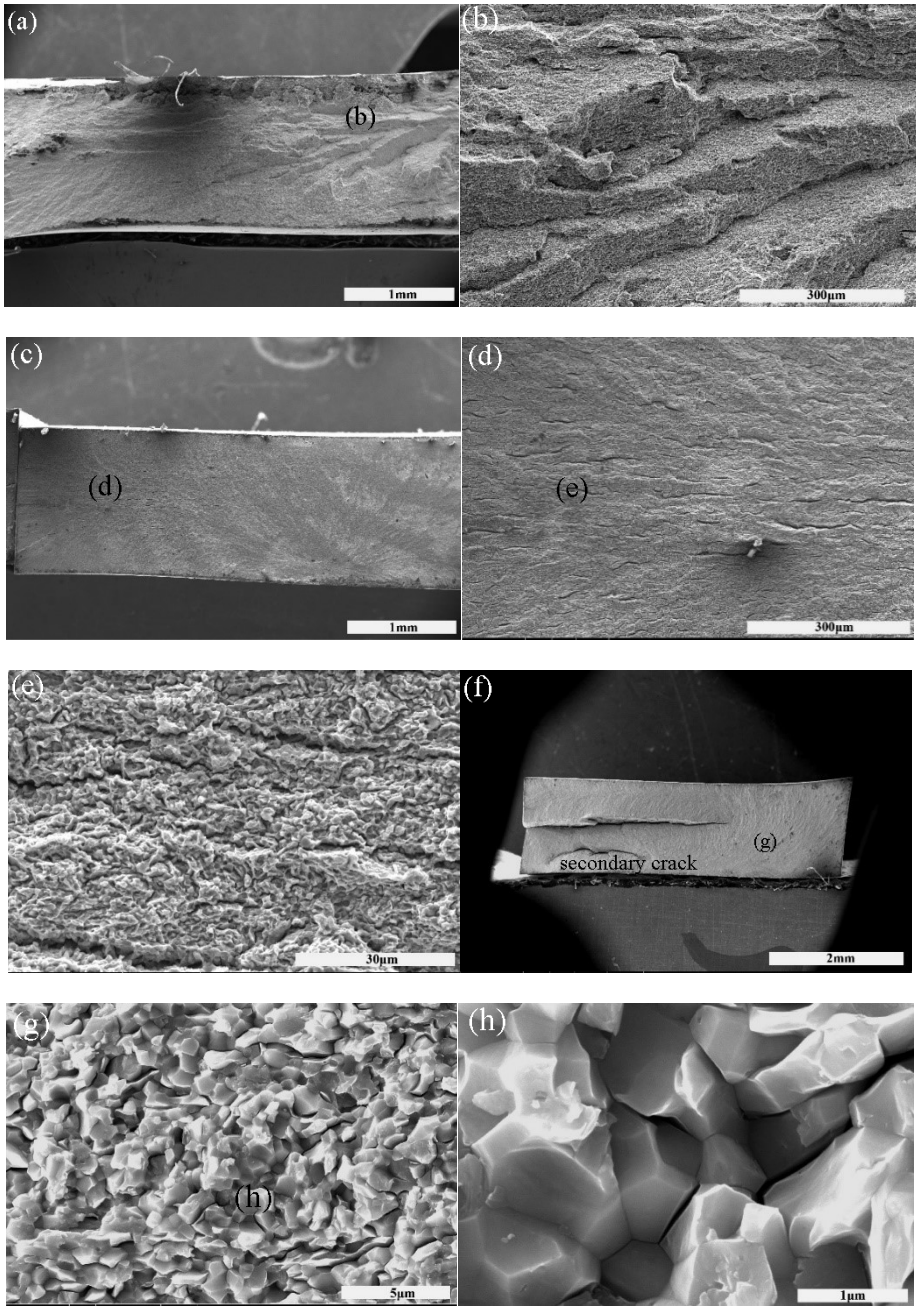

Fig 6 SEM images for M7B obtained under dynamic hydrogen charging constant load test at different pre-strain:(a)0% pre-strain;(b) enlarged regions labelled as b in (a);(c)5% pre-strain;(d) enlarged regions labelled as d in (c);(e) enlarged regions labelled as e in (d);(f)15% pre-strain;(g) enlarged regions labelled as g in (f);(h) enlarged regions labelled as h in (g)

Fig. 6 presents the fracture SEM images of M7B steel under different pre-strain and load conditions. At the edge of the fracture, the divergence texture and

quasi-cleavage steps can be observed clearly. As pre-strain increases from 0 to 0.05, more parallel secondary cracks and microcracks can be observed on the fracture surface in Figs 6(d)(e)(f). As shown, intergranular and transgranular fractures can be clearly seen between the grains. Compared with the tensile fracture in air, fractures after hydrogen charging show an obvious brittle fracture mode, which indicates that the entry of hydrogen reduces the bonding force between grains, deteriorating the mechanical properties of the material.

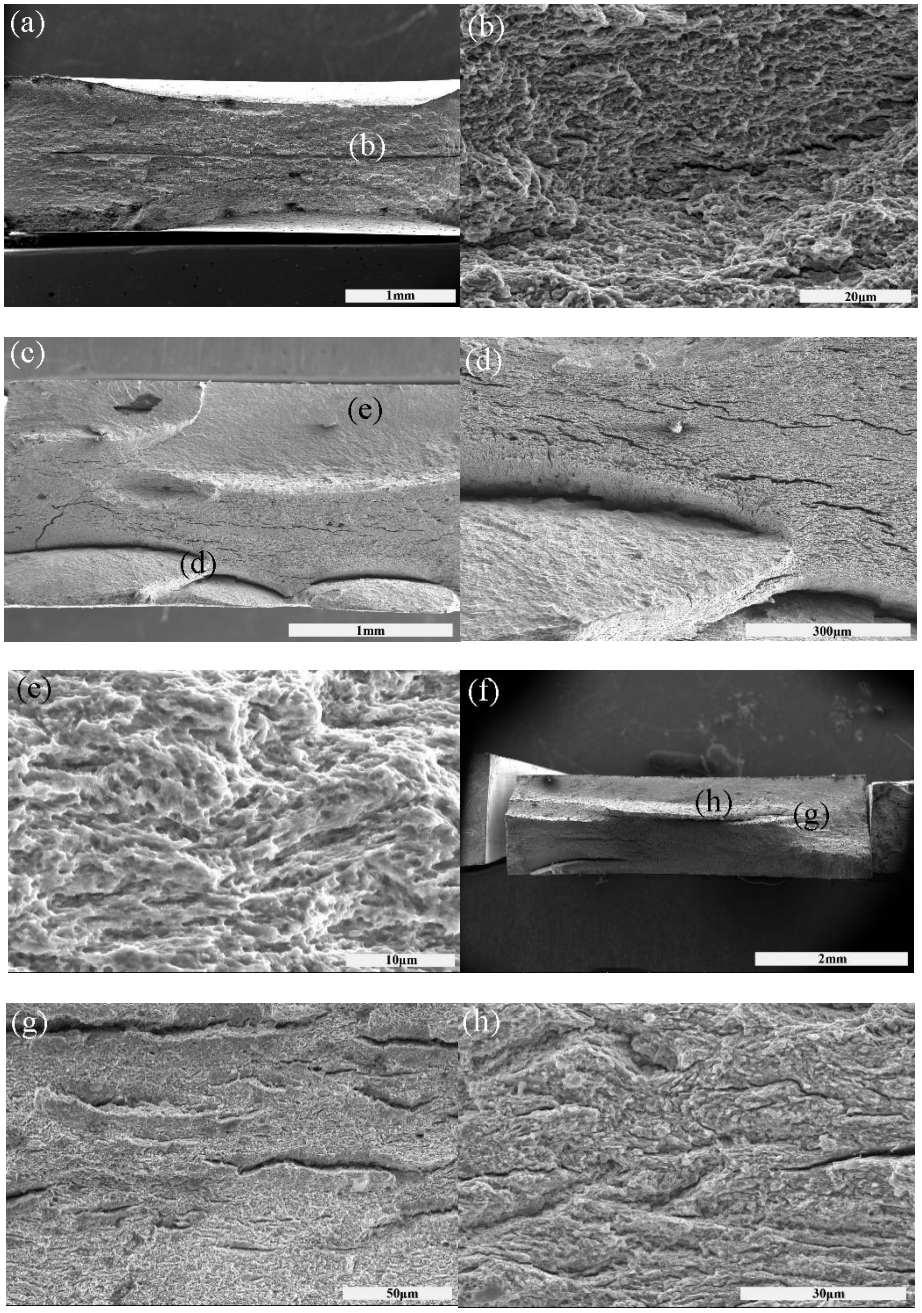

Fig 7 SEM images for M7C obtained under dynamic hydrogen charging constant load test at different pre-strain:(a)0% pre-strain;(b) enlarged regions labelled as b in (a);(c)5% pre-strain;(d), (e) enlarged regions labelled as d, e in (c);(f)15% pre-strain;(g), (h) enlarged regions labelled as g, h in (f)

Fig. 7 shows the fracture SEM image of M7C steel under different pre-strain and

load conditions. Due to the decrease of the cross-sectional area and the rapid crack induced by local stress concentration after local fracture, a portion of the dimple zone is observed in the central region. The corresponding feature areas were selected for magnification of the macrofracture surface of M7C. As can be seen above, the fracture appears clearly at the radical centre. As pre-strain increases, more secondary cracks and microcracks can be observed at the fracture surface in Figs 6(c)(g).

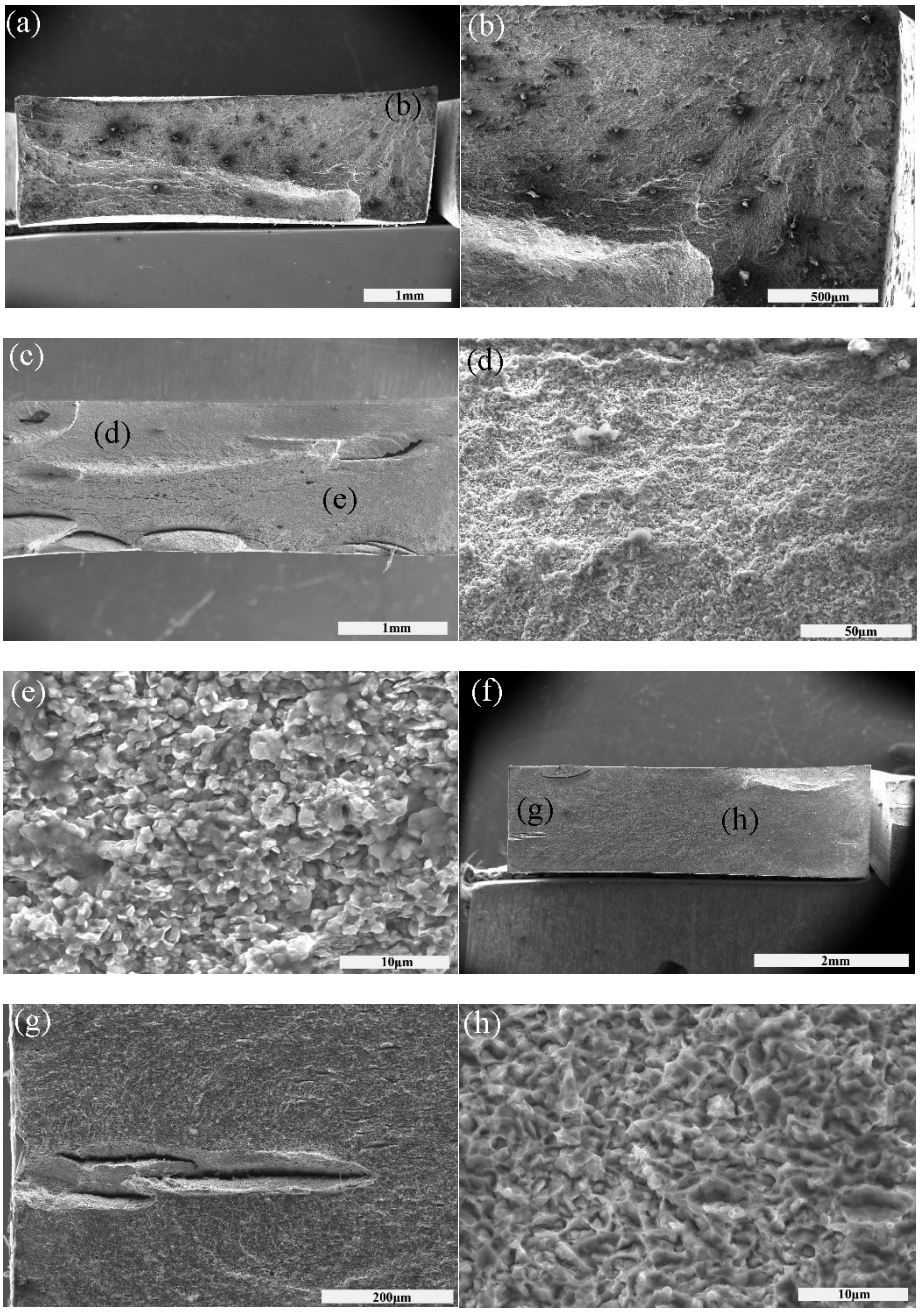

Fig 8 SEM images for M10B obtained under dynamic hydrogen charging constant load test at different pre-strain:(a)0% pre-strain;(b) enlarged regions labelled as b in (a);(c)5% pre-strain;(d), (e) enlarged regions labelled as d, e in (c);(f)15% pre-strain;(g), (h) enlarged regions labelled as g, h in (f)

Fig. 8 contains the fracture SEM image of M10B steel under different pre-strain and load conditions. The fracture features of M10B are similar to those of M7B.

Many secondary cracks were found on the fracture surface, indicating that there were many microcracks in the interior induced by the combined action of hydrogen charging and loading for a long period of time. The origin of the fracture is often at the edge of it, and intergranular or even transgranular fracture characteristics can be observed at high magnification in the local region.

Among the three kinds of MMSs, the normalised threshold stress σ/σ_b of M7B and M10B is much higher than that of M7C when no pre-strain is applied, which is mainly due to the different heat treatment processes of the material. Lengthy batch annealing for M7B and M10B revealed internal defects. The lengthy diffusion of C and Mn elements leads to the improvement of austenite stability and better delayed fracture resistance. The normalised threshold stress of M7B and M10B decreases sharply after applying 0.05 and 0.15 pre-strain. For M7B and M10B, there is a yielding plateau on the stress-strain curve, corresponding to the Lüders band. Currently, the main factor causing local stress concentration is ferrite plastic deformation. The Lüders band, caused by pre-strain in M7B and M7C, not only affects the surface condition of the material, but also increases its susceptibility to hydrogen embrittlement. Because the threshold stress of M7C is not high, it increases slightly due to the increase of pre-strain. By observing the SEM fractographs, the fracture surface of MMSs showed intergranular and transgranular fracture characteristics.

4. Conclusions

The effect of pre-strain on hydrogen-induced delayed cracking for three kinds of medium manganese steel, M7B, M7C and M10B, was studied through immersion and constant load tests. Conclusions are as follows:

Lengthy batch annealing leads to the full recrystallisation of martensite while it reverts to austenite, while long-strip austenite can be combined into block austenite. Continuous annealing for 1–3 minutes can promote the transformation of martensite into austenite, but its microstructure still retains the characteristics of lath martensite.

The different content of Mn indicates the different fraction of austenite. The volume fraction of M10B is higher than that of M7B, showing higher elongation. The threshold stress and hydrogen concentration of medium Mn steels are determined by constant load testing under different strain conditions. The normalised threshold stress factor of M7B and M10B is much higher than that of M7C without pre-strain, which is mainly related to the defects in annealed materials. Upon applying a certain pre-strain, however, the threshold values of M7B and M10B decrease rapidly, which is mainly related to the defects brought about by Lüders strain.

By observing the morphology and fracture in SEM, microcracks were found on all sides, which gradually propagated to the interior of the specimens and initiated the

fracture.

Funding

This work was supported by the National Natural Science Foundation of China [grant number U1760203].

References

[1] R.L. Miller, Ultrafine-grained microstructures and mechanical properties of alloy steels, Metallurgical Transactions 3(4) (1972) 905-912.
[2] T. Furukawa, Dependence of strength–ductility characteristics on thermal history in lowcarbon, 5 wt-%Mn steels, Materials Science and Technology 5(5) (1989) 465-470.
[3] B. Sun, N. Vanderesse, F. Fazeli, C. Scott, J. Chen, P. Bocher, M. Jahazi, S. Yue, Discontinuous strain-induced martensite transformation related to the Portevin-Le Chatelier effect in a medium manganese steel, Scripta Materialia 133 (2017) 9-13.
[4] J.P. Hirth, Effects of hydrogen on the properties of iron and steel, Metallurgical Transactions A 11(6) (1980) 861-890.
[5] H.K. Birnbaum, P. Sofronis, Hydrogen-enhanced localized plasticity—a mechanism for hydrogen-related fracture, Materials Science & Engineering A 176(1-2) (1994) 191-202.
[6] A. Nagao, C.D. Smith, M. Dadfarnia, P. Sofronis, I.M. Robertson, The role of hydrogen in hydrogen embrittlement fracture of lath martensitic steel, Acta Materialia 60(13–14) (2012) 5182-5189.
[7] M. Nagumo, T. Yagi, H. Saitoh, Deformation-induced defects controlling fracture toughness of steel revealed by tritium desorption behaviors, Acta Materialia 48(4) (2000) 943-951.
[8] M. Nagumo, Hydrogen related failure of steels â□□ a new aspect, Metal Science Journal 20(8) (2013) 940-950.
[9] G. Domizzi, G. Anteri, J. Ovejero-GarcíA, Influence of sulphur content and inclusion distribution on the hydrogen induced blister cracking in pressure vessel and pipeline steels, Corrosion Science 43(2) (2001) 325-339.
[10] T. Zhang, W.Y. Chu, K.W. Gao, L.J. Qiao, Study of correlation between hydrogen-induced stress and hydrogen embrittlement, Materials Science and Engineering: A 347(1) (2003) 291-299.
[11] S. Lee, S.J. Lee, B.C.D. Cooman, Austenite stability of ultrafine-grained transformation-induced plasticity steel with Mn partitioning, Scripta Materialia 65(3) (2011) 225-228.
[12] D. Ji, M. Zhang, D. Zhu, S. Luo, L. Li, Influence of microstructure and pre-straining on the bake hardening response for ferrite-martensite dual-phase steels of different grades, Materials Science and Engineering: A 708 (2017) 129-141.
[13] Y. Zhang, L. Wang, K.O. Findley, J.G. Speer, Influence of Temperature and Grain Size on Austenite Stability in Medium Manganese Steels, Metallurgical & Materials Transactions A 48(5) (2017) 1-10.

[14] M. Wang, E. Akiyama, K. Tsuzaki, Determination of the critical hydrogen concentration for delayed fracture of high strength steel by constant load test and numerical calculation, Corrosion Science 48(8) (2006) 2189-2202.
[15] L. Luo, W. Li, L. Wang, S. Zhou, X. Jin, Tensile behaviors and deformation mechanism of a medium Mn-TRIP steel at different temperatures, Materials Science and Engineering: A 682 (2017) 698-703.
[16] M. Calcagnotto, D. Ponge, E. Demir, D. Raabe, Orientation gradients and geometrically necessary dislocations in ultrafine grained dual-phase steels studied by 2D and 3D EBSD, Materials Science and Engineering: A 527(10) (2010) 2738-2746.
[17] L.P. Kubin, A. Mortensen, Geometrically necessary dislocations and strain-gradient plasticity: a few critical issues, Scripta Materialia 48(2) (2003) 119-125.
[18] A. Ghaheri, A. Shafyei, M. Honarmand, Effects of inter-critical temperatures on martensite morphology, volume fraction and mechanical properties of dual-phase steels obtained from direct and continuous annealing cycles, Materials & Design (1980-2015) 62 (2014) 305-319.
[19] J. Han, J.-H. Nam, Y.-K. Lee, The mechanism of hydrogen embrittlement in intercritically annealed medium Mn TRIP steel, Acta Materialia 113 (2016) 1-10.
[20] Z.H. Cai, H. Ding, R.D.K. Misra, Z.Y. Ying, Austenite stability and deformation behavior in a cold-rolled transformation-induced plasticity steel with medium manganese content, Acta Materialia 84 (2015) 229-236.
[21] P.J. Gibbs, E.D. Moor, M.J. Merwin, B. Clausen, J.G. Speer, D.K. Matlock, Austenite Stability Effects on Tensile Behavior of Manganese-Enriched-Austenite Transformation-Induced Plasticity Steel, Metallurgical & Materials Transactions A 42(12) (2011) 3691-3702.